Applied Catalysis A: General, 83 (1992) 179–200
Elsevier Science Publishers B.V., Amsterdam

APCAT 2237

Surface modified niobium oxide catalyst: synthesis, characterization, and catalysis

Jih-Mirn Jehng, Andrzej M. Turek[1] and Israel E. Wachs

Zettlemoyer Center for Surface Studies, Department of Chemical Engineering, Lehigh University, Bethlehem, PA 18015 (USA)

(Received 26 September 1991, revised manuscript received 12 December 1991)

Abstract

The molecular structures and reactivity of surface modified niobium oxide catalysts were determined by Raman spectroscopy, pyridine adsorption as well as the methanol oxidation reaction. Metal oxides (Re_2O_7, CrO_3, WO_3, MoO_3, and V_2O_5) and acids (phosphate and sulfate) form a surface overlayer on the niobia support, and possess a structure similar to the metal oxide ionic species present in acidic solutions (ReO_4^-, $Cr_3O_{10}^{2-}$, $W_{12}O_{40}^{8-}$, $Mo_8O_{26}^{4-}$, $V_{10}O_{28}^{6-}$, $H_2PO_4^-$, and HSO_4^-) when the surface is hydrated. Upon dehydration, only one dehydrated surface ReO_4 species is present on niobia. For the CrO_3, WO_3, MoO_3, V_2O_5, P_2O_5, and sulfate supported on niobia two dehydrated surface metal oxide species, highly distorted and slightly distorted structures, are present. Acidity and BET studies reveal that the presence of the surface metal oxide species stabilizes the surface acidic properties and surface area of niobia during high calcination temperatures (500°C). The 1% V_2O_5 and 1% P_2O_5 on Nb_2O_5 samples possess a high concentration of surface acid sites as well as surface area, and the strength of surface Lewis acid sites on 1% P_2O_5/Nb_2O_5 is stronger than the other systems. In addition, the surface V_2O_5, MoO_3, CrO_3, and Re_2O_7 sites on niobia behave as redox sites and the surface WO_3, P_2O_5, and sulfate sites on niobia behave as acid sites during methanol oxidation. The weak interaction between the surface rhenia species and the niobia support results in volatilization of surface rhenia during methanol oxidation and a corresponding low activity. Thus, the surface properties of niobia catalysts could be altered by the addition of surface metal oxide overlayer.

Keywords: acidity, Fourier-transform infrared spectroscopy, methanol oxidation, niobium oxide, Raman spectroscopy, surface modification.

INTRODUCTION

Niobium oxide has been used as an oxide support for metals such as Ru, Rh, and Ni [1–3] and such catalytic systems exhibit higher alkene selectivity during carbon monoxide hydrogenation compared to conventional oxide supports

Correspondence to: Professor I.E. Wachs, Zettlemoyer Center for Surface Studies, Department of Chemical Engineering, Lehigh University, Bethlehem, PA 18015, USA. Tel. (+1-215)7584274, fax. (+1-215)7583079.
[1]On leave from Faculty of Chemistry, Jagiellonian University, Cracow, Poland.

such as alumina and silica. Metal oxides can also be deposited on niobia by reaction with the surface hydroxyl groups of the oxide support to form new surface metal oxide phases [4]. These surface metal oxide phases have been found to enhance the chemical and physical properties of the supported metal oxide catalysts. The interaction between the surface metal oxide and the oxide support strongly affects the surface metal oxide structure. The different surface metal oxide states result in different catalytic behavior, and the overall catalytic activity and selectivity are also dependent on the surface concentration of these surface metal oxide species. For example, niobium oxide promotes the catalytic properties of the niobia supported vanadium and molybdenum oxide phases during the dehydration of isopropanol to propene [5,6] and the partial oxidation of methanol [7]. However, the niobia support used in the previous studies possessed a low surface area (<30 m^2/g) compared to conventional oxide supports (TiO_2, SiO_2, and Al_2O_3), and the relationships between the molecular structures of the surface metal oxide species on niobia and their reactivity are not well understood.

Hydrated niobium oxide, $Nb_2O_5 \cdot nH_2O$, is known to be a new type of strong solid acid exhibiting high catalytic activity and selectivity for hydration of alkenes, dehydration of alcohols, esterification of carboxylic acids with alcohols, and condensation of butylaldehyde [8–13]. Acidity measurements have shown that strong Lewis and Brønsted acid sites are present on hydrated niobium oxide when it is treated at 120–300°C. The acidity and catalytic activity, however, decrease dramatically at high temperature treatments (>400°C) due to loss in surface area, removal of water, and crystallization of the hydrated niobium oxide structure.

In the present study, hydrated niobium oxide calcined at 120°C for 24 h and possessing a surface area of ca. 120 m^2/g was used as a support for preparing the surface modified niobium oxide catalysts. The surface modified niobium oxide catalysts were prepared by depositing metal oxides (Re_2O_7, CrO_3, WO_3, MoO_3, and V_2O_5) and acids (sulfate and phosphate) on the niobia support. The surface areas of these catalysts were measured after calcination by the BET method as a function of metal oxide loading. The molecular structures of the surface metal oxide overlayers on the niobia support, both under ambient and in situ conditions, were characterized by Raman spectroscopy as a function of metal oxide loading. The surface acidity and reactivity of the surface modified niobium oxide catalysts were investigated with Fourier-transform infrared spectroscopy (FT-IR) pyridine adsorption and the methanol oxidation reaction. The structure–reactivity relationships of the surface modified niobium oxide catalysts can be established by combining the structural information with the acidity and catalytic data.

EXPERIMENTAL

Materials and preparations

Hydrated niobium oxide ($Nb_2O_5 \cdot nH_2O$) was provided by Niobium Products Company (Pittsburgh, PA) with a minimum purity of 99.0%. The major impurities after calcination at 800°C are 0.02% Ta and 0.01% Cl. The precursors used in the preparation of the surface modified niobium oxide catalysts were: perrhenic acid, $HReO_4$ 99.99% (Aldrich, Milwaukee, WI); chromium nitrate, $Cr(NO_3)_3 \cdot 9H_2O$ 98.5% (Baker & Adamson, Morristown, NJ); ammonium metatungstate, $(NH_4)_6H_2W_{12}O_{40} \cdot xH_2O$ 99.9% (Pfaltz & Bauer, Waterbury, CT); ammonium heptamolybdate, $(NH_4)_6Mo_7O_{24} \cdot 4H_2O$ 99.9% (Alfa, Danvers, MA); vanadium triisopropoxide, $VO(OC_3H_7)_3$ 95–99% (Johnson Matthey, Ward Hill, MA); phosphoric acid 85%, H_3PO_4, and sulfuric acid, H_2SO_4 95–98% (Fisher Scientific, Fair Lawn, NJ).

The catalysts were prepared by the incipient-wetness impregnation method. For the non-air sensitive precursors, metal oxide salts and acids were dissolved in distilled water and then impregnated into the niobia support. The wet samples were then dried at the room temperature for 16 h and further dried at 120°C for 16 h to remove the excess water. After the drying procedure, the samples were calcined at 500°C for 2 h to decompose the salt ligands to form the surface modified niobium oxide catalysts. For the air sensitive precursors, the metal oxide salt/methanol solution was impregnated into the niobia support under a nitrogen environment to avoid the crystallization of the precursor with ambient moisture, and the impregnated samples were kept in a glove box for several hours to evaporate the excess alcohol. The samples were subsequently dried at 120°C for 16 h under flowing nitrogen gas in an oven. The dried samples were then calcined at 500°C under the nitrogen gas for the first hour then switched to the oxygen gas for the second hour.

BET surface area measurement

The BET surface areas of bulk niobium oxide samples were obtained with a Quantsorb surface area analyzer (Quantachrome corporation, Model OS-9) using a 3:7 ratio of N_2/He mixture as a probe gas. Typically, 0.200–0.300 g of sample was used for the measurement and the sample was outgassed at 250°C prior to nitrogen adsorption.

Raman spectroscopy

Raman spectra were obtained with a Spex triplemate spectrometer (Model 1877) coupled to an EG&G intensified photodiode array detector which was cooled thermoelectrically to −35°C, and interfaced with an EG&G OMA III

Optical Multichannel Analyzer (Model 1463). The samples were excited by the 514.5 nm line of the Ar^+ laser with 10–100 mW power. The laser beam was focused on the sample illuminator, where the sample typically spins at about 2000 rpm to avoid local heating, and was reflected into the spectrometer by a 90° angle with the incident light. The scattered Raman light was collected by the spectrometer at room temperature, and analyzed with an OMA III software package. The Raman spectra of the surface modified niobium oxide catalysts was only collected in the high wavenumber region (700–1200 cm^{-1}) due to the strong Raman scattering from the niobia support in the low wavenumber region (<700 cm^{-1}). The weak niobium oxide Raman features in the 700–1200 cm^{-1} region were also subtracted from the spectra in order to observe more clearly the Raman features of the surface metal oxide species. The overall spectral resolution of the spectra was determined to be about 2 cm^{-1}. The detailed schematic diagram of the Raman spectrometer is described elsewhere [14].

An in situ quartz cell was designed in order to investigate the structural changes upon dehydration of the surface modified niobium oxide samples above room temperature. The sample holder was made from quartz glass, and the sample disc was held by a stationary slot in the sample holder. The sample was first calcined at 450°C for 2 h under flowing dry air in an oven, and then transferred into the in situ cell which was heated by a cylindrical heating coil under flowing oxygen. After the cell had been heated to about 400°C for 30 min, it was removed from the heating coil and cooled down to room temperature. The dehydrated Raman spectra were immediately collected at the room temperature.

Acidity measurements

The surface acidity of the surface modified niobium oxide catalysts was measured with an Analect FX-6160 FT-IR spectrometer by pyridine adsorption. The samples were pressed into a thin wafer (10–30 mg/cm^{-2}) and evacuated in an IR cell at 425°C for 1 h. Upon cooling the cell to 200°C, the IR spectrum (A) was recorded. Pyridine vapor was then introduced into the cell with a pressure of 5 Torr (1 Torr = 133.3 Pa), and adsorbed on the sample for about 30 s. Subsequently, physically adsorbed pyridine was desorbed by evacuating the sample for 15 min, and the pyridine adsorption IR spectrum (B) was recorded again. The concentration of Brønsted and Lewis acid sites were calculated from the intensities of PyH^+ (ca. 1540 cm^{-1}) and PyL (ca. 1450 cm^{-1}) bands with their corresponding extinction coefficients after subtracting spectrum A from B [15,16].

Catalysis studies

Catalysis studies on the surface modified niobium oxide catalysts were performed with the sensitive methanol oxidation reaction in order to study the

surface chemistry of these catalysts. The reactor consists of a digital flow-rate controller (Brooks), a tube furnace (Lindberg), a condenser and methanol reservoir, and a gas chromatograph (HP 5840). A portion of the methanol in the bottom flask was constantly evaporated under a controlled temperature and pressure. The evaporated methanol was mixed with the helium and oxygen gases whose flow-rates were adjusted by the mass flow-rate controller. This mixed gas flowed through the condenser at a temperature of 9.6°C. The 6.9:11.0:82.1 ratio of a $CH_3OH/O_2/He$ mixture gas then flowed to the catalysts. The gas flow-rate was maintained at 50–100 sccm in order to keep a low conversion of 5 mol-%. The catalysts with an average particle size of 75 μm were placed in the center of a 6-mm O.D. Pyrex microreactor supported by glass wool. The reactor was heated up by a programmable tube furnace to a constant reaction temperature of 230°C. The effluent gases were analyzed by an online gas chromatograph. The gas chromatograph has been modified to operate with two thermal conductivity detectors (TCD) and one flame ionization detector (FID) with two packed columns (Poropak R and Carbosieve SII), and programmed to perform automatic data acquisition and analysis. The catalytic activity and selectivity were obtained by integrating the peak areas of products with respect to the reference peak area of methanol.

RESULTS AND DISCUSSION

BET surface area

It is known that the surface area of hydrated niobium oxide dramatically decreases with increasing calcination temperature due to the formation of large Nb_2O_5 crystals from the heat treatment [17]. The thermal phase transformations of bulk niobia were determined by Raman and XRD, and the corresponding shift of the Raman band from ca. 650 to ca. 690 cm^{-1} is due to the transformation of amorphous Nb_2O_5 (120°C) to crystalline TT-Nb_2O_5 (500°C) [17]. The surface areas of metal oxides (V_2O_5, MoO_3, Re_2O_7, CrO_3, and WO_3) and acids (H_2SO_4 and H_3PO_4) supported on niobia after a 500°C calcination treatment, which are based on gram of sample, are shown in Figs. 1 and 2 as a function of metal oxide and acid loading, respectively. At low metal oxide loadings (less than 10 wt.-%), the surface areas of the resultant supported metal oxide catalysts has the following order: $V_2O_5/Nb_2O_5 > CrO_3/Nb_2O_5 > WO_3/Nb_2O_5 > MoO_3/Nb_2O_5 > ReO_3/Nb_2O_5 > Nb_2O_5$. Thus, the surface area of niobium oxide at elevated calcination temperatures depends on the nature of surface metal oxide species present. The surface area of niobium oxide was also stabilized by supported phosphate and sulfate at low loadings. At high loadings, the surface area of the sulfated niobium oxide decreased faster than that of the phosphated niobium oxide as shown in Fig. 2. Comparison of the slope of surface area vs. surface coverage of the surface modified niobium

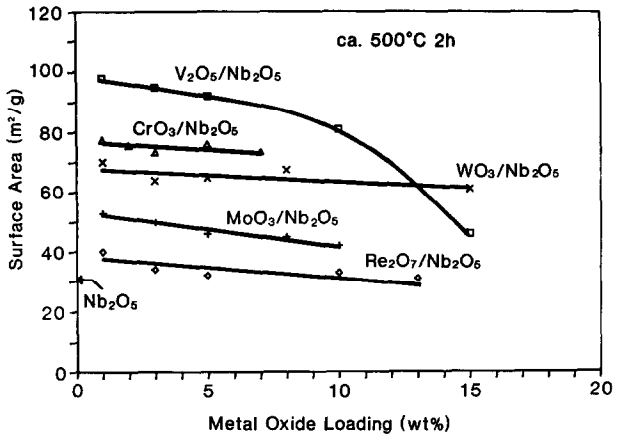

Fig. 1. The surface areas of surface modified niobium oxde catalysts as a function of metal oxide loading.

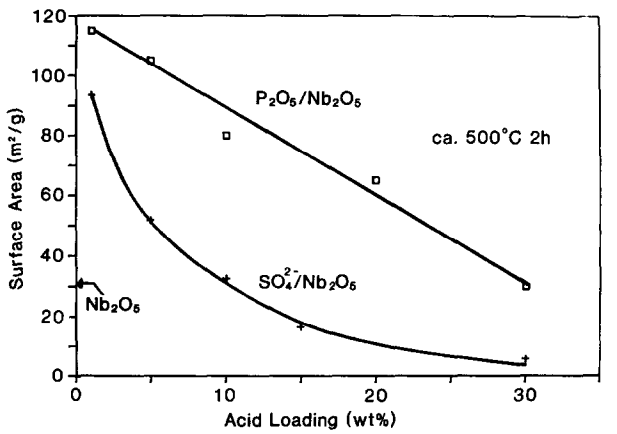

Fig. 2. The surface areas of surface modified niobium oxide catalysts as a function of acid loading.

oxide catalysts at the loading below 10 wt.-% in Figs. 1 and 2 reveal that the surface metal oxide phases retain the niobium oxide surface better than the surface acid phases.

The various deposited metal oxides exhibit a different interaction with the surface hydroxyl groups of niobium oxide and inhibit the dehydroxylation of niobium oxide [18,19]. For example, the surface vanadium oxide species strongly interact with the niobia support and retain a high surface area for the V_2O_5/Nb_2O_5 system and exhibits a Raman band at ca. 650 cm^{-1} characteristic of amorphous Nb_2O_5 [17]. However, the surface rhenium oxide species weakly interact with the niobia support and results in a low surface area for the Re_2O_7/Nb_2O_5 system with a Raman band at ca. 690 cm^{-1} characteristic of crystalline

TT-Nb_2O_5 [17]. The addition of low amounts of phosphoric acid can also inhibit the phase transformation of niobium oxide at high calcination temperatures (>500°C) as well as retain the surface acidic properties for catalytic reactions [20–22]. However, a high concentration of the surface sulfate species does not stabilize the Nb_2O_5 surface area at 500°C calcination temperature, and the dissolution of niobium oxide into a strong sulfuric acid solution can occur.

Raman spectra of surface modified niobium oxide catalysts under ambient conditions

Re_2O_7/Nb_2O_5

The ambient Raman spectra of 1–10 wt.-% Re_2O_7/Nb_2O_5 samples treated at 500°C for 2 h are shown in Fig. 3. The Raman band at ca. 979 cm^{-1} is characteristic of the surface rhenia species present on the niobia support [23]. The slight shift of the Raman band from ca. 979 cm^{-1} to 989 cm^{-1} upon increasing rhenia loading is probably due to a slight increase in the Re=O bond order or possibly the subtraction of the niobia support Raman signal. A very weak and broad Raman band at ca. 900 cm^{-1} is also observed. Comparison of the Raman features of the Re_2O_7/Nb_2O_5 system with that of the tetrahedral perrhenate ion in aqueous solutions [23,24] suggests that the surface rhenia species possess a tetrahedral ReO_4 structure with the symmetric and asymmetric stretching modes appearing at ca. 980 and ca. 900 cm^{-1}, respectively.

Recent studies on the Re_2O_7/Al_2O_3 catalysts have revealed that the maximum loading of rhenia on alumina (ca. 180 m^2/g) was achieved at ca. 14 wt.-% Re_2O_7/Al_2O_3, which is significantly less than a complete monolayer (calculated to be at 18–20 wt.-% Re_2O_7/Al_2O_3), due to the recombination and de-

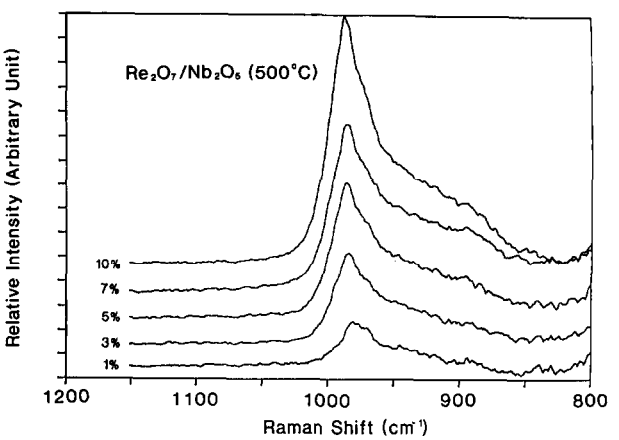

Fig. 3. The Raman spectra of Re_2O_7 supported on niobium oxide as a function of Re_2O_7 loading.

sorption of the $[ReO_4]_{ads}$ species into gaseous Re_2O_7 molecules at high surface coverages [23]. The desorption of gaseous Re_2O_7 molecules on oxide supports prevents the formation of a complete monolayer for the Re_2O_7/Nb_2O_5 system (which is expected to be ca. 6 wt.-% Re_2O_7/Nb_2O_5) from Raman spectroscopy.

CrO_3/Nb_2O_5

The Raman spectra of 2–7 wt.-% CrO_3/Nb_2O_5 samples calcined at 500°C are shown in Fig. 4. The 2 wt.-% CrO_3/Nb_2O_5 sample possesses a broad Raman band at ca. 900 cm^{-1} characteristic of the vibrational mode of the surface chromium oxide species [25]. Additional Raman bands at ca. 985, ca. 965, and ca. 830 cm^{-1} are observed for higher CrO_3 loadings and are also characteristic of surface chromium oxide species [25]. Raman results of the CrO_3/Nb_2O_5 catalysts indicate that the surface chromium oxide species (Raman bands at ca. 985, ca. 965, ca. 900, and ca. 830 cm^{-1}) possess a polymeric structure which is similar to a $Cr_3O_{10}^{2-}$ cluster present in aqueous acidic solutions [25–27].

In addition, the Raman spectrum of 7 wt.-% CrO_3/Nb_2O_5 (500°C) in the 100–1200 cm^{-1} region exhibits a new band at ca. 550 cm^{-1} which indicates the presence of Cr_2O_3 crystallites on the niobia surface, and suggests that monolayer coverage of the surface chromium oxide overlayer on the niobia support is achieved below 7 wt.-% CrO_3/Nb_2O_5. This is in agreement with the expected monolayer coverage of the supported chromium oxide on niobia with ca. 80 m^2/g surface area which is calculated to be ca. 6 wt.-% CrO_3/Nb_2O_5 on the basis of monolayer coverage of ca. 14 wt.-% CrO_3 on alumina with ca. 180 m^2/g surface area [25].

WO_3/Nb_2O_5

The Raman spectra of 1–15 wt.-% WO_3/Nb_2O_5 calcined at 500°C are shown in Fig. 5. Weak and broad bands at ca. 980 and ca. 880 cm^{-1} are characteristic

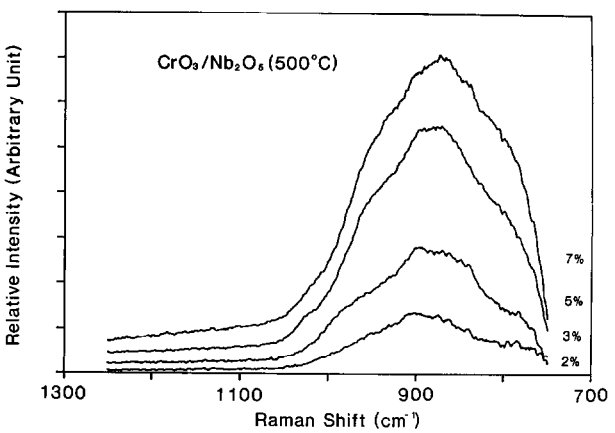

Fig. 4. The Raman spectra of CrO_3 supported on niobium oxide as a function of CrO_3 loading.

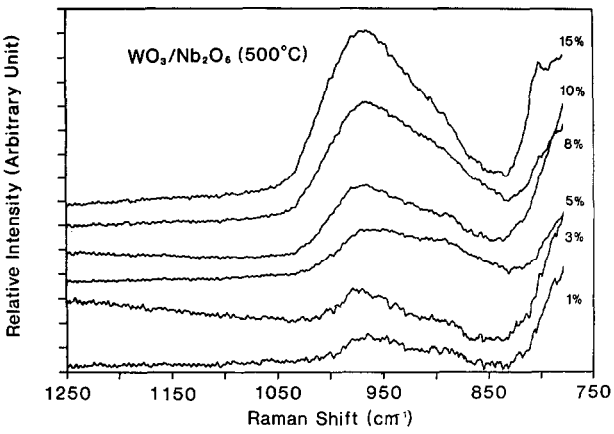

Fig. 5. The Raman spectra of WO_3 supported on niobium oxide as a function of WO_3 loading.

of the surface tungsten oxide species [28,19], and the intensity of these bands increases with increasing tungsten oxide loading. Raman results of the WO_3/Nb_2O_5 catalysts indicate that the surface tungsten oxide species (Raman bands at ca. 980 and ca. 880 cm^{-1}) are present as a polymeric structure which is consistent with the $W_{12}O_{40}^{8-}$ clusters present in aqueous acidic solutions [26,29].

For the 15 wt.-% WO_3/Nb_2O_5 sample, a weak and sharp Raman band appearing at ca. 805 cm^{-1} suggests that monolayer coverage of the surface tungsten oxide overlayer on niobia possessing ca. 70 m^2/g surface area is achieved below 15 wt.-% WO_3/Nb_2O_5. This is consistent with the expected monolayer coverage of the surface tungsten oxide overlayer on niobia which is ca. 12 wt.-% WO_3/Nb_2O_5 on the basis of ca. 30 wt.-% WO_3/Al_2O_3 (180 m^2/g) monolayer coverage [28].

MoO_3/Nb_2O_5

The Raman spectra of 1–10 wt.-% MoO_3/Nb_2O_5 samples are presented in Fig. 6 and show a broad and strong Raman band at ca. 960 cm^{-1} which is assigned to the vibrational mode of the surface molybdenum oxide species present on the niobia support [30]. Raman studies on the MoO_3/Nb_2O_5 catalysts indicate that the surface MoO_3 species (Raman band at ca. 960 cm^{-1}) are present as a polymeric structure which is consistent with the $Mo_8O_{26}^{4-}$ clusters present in aqueous acidic solutions [26,30].

Monolayer coverage of the supported molybdenum oxide on niobia with ca. 40 m^2/g surface area is calculated to be ca. 4 wt.-% MoO_3/Nb_2O_5 on the basis of monolayer coverage of 18 wt.-% MoO_3 on alumina with ca. 180 m^2/g surface area [31]. However, crystalline MoO_3 Raman bands at ca. 997 and ca. 820 cm^{-1} are not observed in the samples containing 5–10 wt.-% MoO_3. The ab-

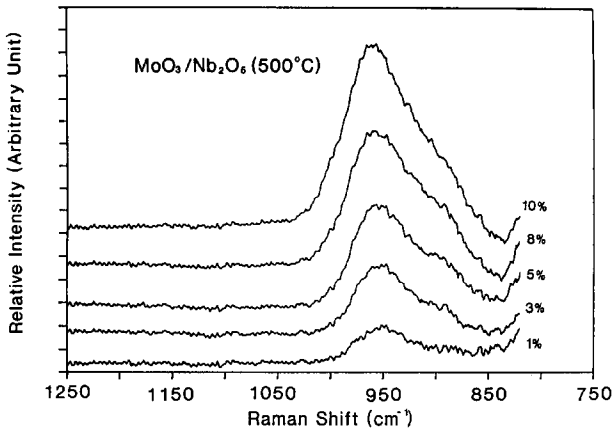

Fig. 6. The Raman spectra of MoO_3 supported on niobium oxide as a function of MoO_3 loading.

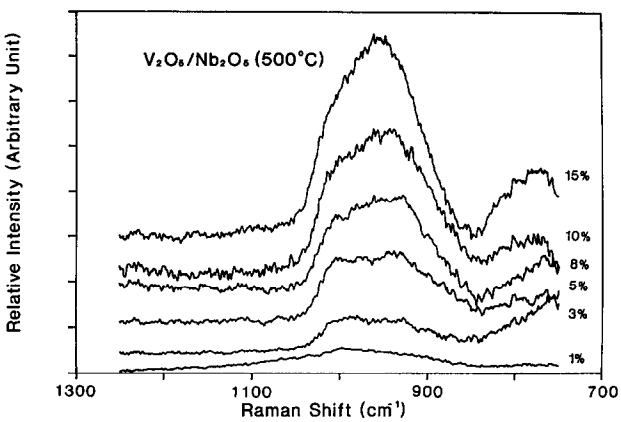

Fig. 7. The Raman spectra of V_2O_5 supported on niobium oxide as a function of V_2O_5 loading.

sence of crystalline MoO_3 phase on niobia for the MoO_3 loadings above 5 wt.-% suggests that molybdenum oxide might be incorporated into the niobia support to form solid solutions.

V_2O_5/Nb_2O_5

The Raman spectra of 1–15 wt.-% V_2O_5/Nb_2O_5 samples calcined at 500°C, shown in Fig. 7, reveal that the crystalline V_2O_5 phase (Raman bands at ca. 994, ca. 702, ca. 527, ca. 404, ca. 284, and ca. 146 cm^{-1}) is not present on the niobia support up to 15 wt.-% V_2O_5 loading. At low V_2O_5 loading (<3 wt.-%), a weak and broad Raman band at ca. 995 cm^{-1} is present and is characteristic of the surface vanadia species on the niobia support [32]. Upon further increasing the vanadia loading (>3 wt.-%), a second vanadia species is present on the niobia support as reflected by the new Raman band observed at ca. 930

cm^{-1}. Raman studies of the V_2O_5 supported on niobia indicate that the surface vanadia species (Raman band at ca. 995 cm^{-1}) are present as a polymeric structure which is similar to the $V_{10}O_{28}^{6-}$ clusters present in aqueous acidic solutions [26,32]. At high vanadia coverages (>3 wt.-%), a second Raman band appears at ca. 930 cm^{-1} which is characteristic of the vibrational mode of a tetrahedral VO_4 structure which is stabilized by Nb_2O_5 bulk since the hydrated surface vanadia species below monolayer coverage only possess an octahedral VO_6 structure (Raman band at ca. 1000 cm^{-1}) in acidic environment [32]. The presence of the tetrahedral VO_4 structure in the V_2O_5/Nb_2O_5 system is also confirmed by ^{51}V solid state wideline NMR [33].

Deo et al. [34] concluded that monolayer coverage of supported vanadia on γ-Al_2O_3 with a surface area ca. 180 m^2/g is reached at ca. 20 wt.-% V_2O_5/Al_2O_3, and monolayer coverage of the supported vanadia on niobia with a surface area ca. 90 m^2/g is estimated to be ca. 10 wt.-% V_2O_5/Nb_2O_5. However, a crystalline V_2O_5 phase is not present in the 15 wt.-% V_2O_5/Nb_2O_5 sample. High resolution ^{51}V NMR studies of the $NbVO_5$ compound indicate that V^{5+} atom is tetrahedrally coordinated and possesses an orthovanadate structure [35]. The V–O bond distance/stretching frequency correlation derived by Hardcastle and Wachs [36] can be used to predict the Raman band positions of the $NbVO_5$ compound. The predicted V–O stretching frequency, corresponding to the bond distances of 1.857, 1.783, and 1.671 Å in $NbVO_5$, would appear at ca. 610, ca. 700, and ca. 870 cm^{-1}, respectively. This suggest that the tetrahedral VO_4 species in the V_2O_5/Nb_2O_5 system contain a somewhat more distorted structure than that in the $NbVO_5$ compound.

P_2O_5/Nb_2O_5 and SO_4^{2-}/Nb_2O_5

Phosphorous and sulfurous compounds generally possess tetrahedrally-coordinated PO_4 and SO_4 units in the structure. Compounds containing 5 or 6 octahedrally-coordinated P and S atoms are relatively few in number [37]. Phosphoric acid in aqueous solution possesses a regular tetrahedral PO_4 structure with Raman bands at ca. 890 and ca. 1170 cm^{-1} which are characteristic of the P–O symmetric and antisymmetric stretching modes of the tetrahedral PO_4 structure, respectively [38], and the aqueous H_2SO_4 species possesses corresponding Raman bands at ca. 918 and ca. 1150 cm^{-1} which are characteristic of the S–O symmetric and antisymmetric stretching modes of the tetrahedral SO_4 structure, respectively.

The Raman spectra of 1–30 wt.-% P_2O_5/Nb_2O_5 and 5–30 wt.-% SO_4^{2-}/Nb_2O_5 are shown in Figs. 8 and 9. For the phosphate (sulfate) supported on niobia at low surface coverages (<5 wt.-%), the Raman studies indicate that the surface phosphate (sulfate) species possess a regular tetrahedral PO_4 (SO_4) structure. At high acid coverages (>10 wt.-%), the shift of the Raman band from ca. 900 to ca. 980 cm^{-1} for the surface phosphate species suggests that a polyphosphate species form on the niobia surface [39], and the surface sulfate species possess a structure similar to the dimeric S_2O_7 species with a broad Raman

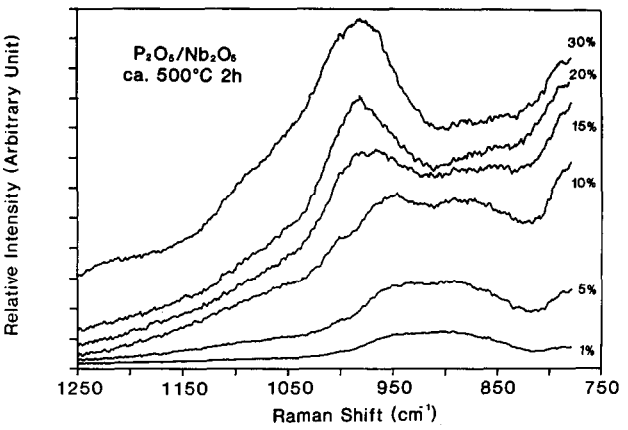

Fig. 8. The Raman spectra of P_2O_5 supported on niobium oxide as a function of P_2O_5 loading.

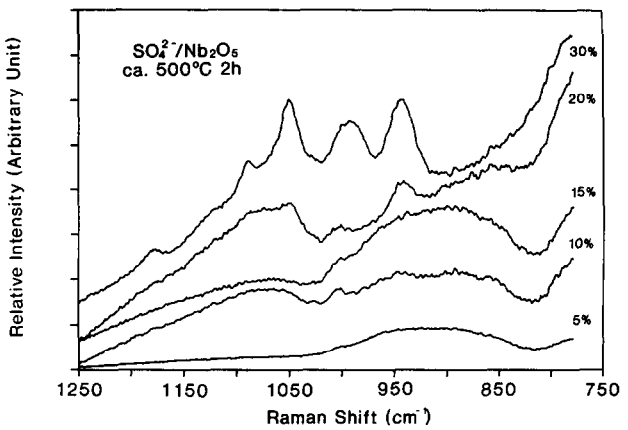

Fig. 9. The Raman spectra of sulfate supported on niobium oxide as a function of sulfate loading.

band at ca. 1070 cm^{-1} [40]. Multiple Raman bands (ca. 940, ca. 995, ca. 1050, ca. 1090, and ca. 1175 cm^{-1}) observed at very high sulfuric acid concentration (30 wt.-%) indicate that a solid Nb–S–O compound may be formed due to the dissolution of niobia into the sulfuric acid solution and the loss of surface area. The presence of the surface phosphate species on the SiO_2, Al_2O_3, and TiO_2 supports was also determined by Busca et al. using TG-DTA, XRD, and FT-IR [41]. They suggest that the surface phosphate species weakly interact with the silica support and form mainly liquid-like H_3PO_4 species containing covalently bonded phosphate as well as hydrogen phosphate species. The surface phosphate species are well dispersed on the Al_2O_3 and TiO_2 support, and form ionically bonded hydrogen phosphate as well as phosphate species [41].

It appears that Raman spectroscopy is a powerful technique for determining

the molecular structures of the surface metal oxide phases [27–33]. XRD can not provide the structural information of a surface metal oxide phase with a particle size smaller than 40 Å, and the surface metal oxide phases are also difficult to detect by TEM. Recent Raman characterization studies of V_2O_5, MoO_3, WO_3, and CrO_3 supported on the Al_2O_3, TiO_2, SiO_2, ZrO_2, and MgO supports under ambient conditions have demonstrated that the molecular structures of the hydrated surface metal oxide phases are directly related to the surface pH of the aqueous film which is determined by the combined pH of the oxide support and the metal oxide overlayer [32]. In aqueous environments, the oxide support equilibrates at the pH which results in net zero surface charge (point of zero charge or isoelectric point). The pH at the point of zero charge of the niobia support is ca. 0.5 [42,43]. For the surface modified niobium oxide catalysts, the point of zero charge of such composite materials is determined by the combined pH of the niobia support and the metal oxide overlayer. Gil-Llambias et al. [44] have shown that the pH at the point zero surface charge of the Al_2O_3 ($pH \approx 9$) supported V_2O_5 and MoO_3 and the TiO_2 ($pH \approx 5$–6) supported V_2O_5 and MoO_3 systems decreases with increasing surface vanadium oxide coverage. The surface pH of the supported vanadium oxide system is expected to be close to the oxide support at low surface coverages, but significantly lower than the surface pH of the Al_2O_3 and TiO_2 supports at high surface coverages because the pH at the point zero surface charge of $V_2O_5 \approx 1.5$.

An examination of the solution chemistry of the various metal oxides in this study reveals that metal oxide clusters are formed in acidic solutions with the exception of rhenium oxide which only forms isolated species [26]. The low pH of the surface modified niobium oxide systems results in the formation of metal oxide clusters on the surface as expected. Consequently, the surface pH of the surface modified niobium oxide catalysts under ambient conditions is significantly influenced by the acidic niobia support. Surface metal oxides and

TABLE 1

The molecular structures of surface modified niobium oxide catalysts under ambient conditions

Modifier	Observed surface metal oxide phases on Nb_2O_5	Predicted metal oxide species in acidic solution
Re	ReO_4	ReO_4^{1-}
Cr	Cr_3O_{10}	$Cr_3O_{10}^{2-}$
Mo	Mo_8O_{26}	$Mo_8O_{26}^{4-}$
W	$W_{12}O_{40}$	$W_{12}O_{40}^{8-}$
V	$V_{10}O_{28}$	$V_{10}O_{28}^{6-}$
P	H_2PO_4	$H_2PO_4^{1-}$
S	HSO_4	HSO_4^{1-}

acids species with that of the predicted metal oxides and acids in acidic solution are listed in Table 1.

Raman spectra of surface modified niobium oxide catalysts under in situ conditions

The molecular structures of the surface modified niobium oxide catalysts below monolayer coverage were further investigated by in situ Raman spectroscopy. Under in situ conditions the adsorbed moisture desorbs upon heating and the surface metal oxides or acids species on the niobia support become dehydrated [14,17,31,45]. Raman shifts upon dehydration provide additional evidence that the supported metal oxide phases are present as surface overlayers on the niobia support [14]. Raman bands of the surface modified niobium oxide catalysts under in situ conditions are tabulated in Table 2.

Upon dehydration treatments, the major Raman band at ca. 980 cm^{-1} for 3 wt.-% Re_2O_7/Nb_2O_5 shifts to ca. 1008 cm^{-1}, and an additional Raman band appears at ca. 976 cm^{-1}. Raman results suggest that only one dehydrated surface rhenium oxide species is present on the niobia surface. Recent Raman and IR studies on the Al_2O_3, ZrO_2, TiO_2, and SiO_2-supported Re_2O_7 catalysts reveal that the dehydrated surface rhenium oxide species possess a tetrahedral ReO_4 structure containing three terminal Re=O bonds and one Re–O–support bridging bond [46]. The Raman bands in the 1015–1004 and 980–890 cm^{-1} are assigned to the symmetric and antisymmetric stretching modes of the dehydrated surface rhenium oxide species. Thus, the Raman bands at ca. 1008 and ca. 976 cm^{-1} for the Re_2O_7/Nb_2O_5 sample (see Table 2) are characteristic of the symmetric and antisymmetric stretching modes of the surface rhenium oxide species possessing a tetrahedral O–Re[=O]$_3$ structure.

For the dehydrated 3 wt.-% CrO_3/Nb_2O_5 sample, a major Raman band at ca. 890 cm^{-1} and two weak Raman bands at ca. 1010 and ca. 966 cm^{-1} are observed. The major Raman bands for 8 wt.-% WO_3/Nb_2O_5, 8 wt.-% $MoO_3/$

TABLE 2

Raman bands of surface modified niobium oxide catalysts under in situ conditions

Catalyst	Raman bands (cm^{-1})
3% Re_2O_7/Nb_2O_5	1008 (s), 976 (w)
3% V_2O_5/Nb_2O_5	1033 (s), 925 (s)
8% MoO_3/Nb_2O_5	1003 (s), 942 (m)
8% WO_3/Nb_2O_5	1018 (m), 956 (s)
3% CrO_3/Nb_2O_5	1010 (w), 966 (w), 890 (s)
5% SO_4^{2-}/Nb_2O_5	1001 (w), 932 (s)
10% P_2O_5/Nb_2O_5	1004 (s), 951 (w), 878 (m)

Nb_2O_5, and 3 wt.-% V_2O_5/Nb_2O_5 shift and split into two bands at ca. 1018 and ca. 956 cm^{-1}, ca. 1003 and ca. 942 cm^{-1}, and ca. 1033 and ca. 925 cm^{-1}, respectively, upon dehydration treatments (see Table 2). The dehydrated Raman spectra of the supported CrO_3, WO_3, MoO_3, and V_2O_5 on the niobia support suggest that multiple dehydrated surface metal oxide species are present on niobium oxide: an isolated highly distorted structure with a short M=O bond in the 1003–1033 cm^{-1} region, and a polymeric structure with a longer M–O bond in the 890–956 cm^{-1} region which does not have a significant perturbation upon dehydration. The molecular structures of Al_2O_3, TiO_2, and SiO_2-supported V_2O_5 catalysts have been extensively characterized by Raman spectroscopy [47–50]. Upon dehydration, the surface vanadium oxide Raman bands above 800 cm^{-1}, which are characteristic of the V=O symmetric stretch, split into a sharp Raman band in the 1026–1038 cm^{-1} region and a broad Raman band at ca. 900 cm^{-1}. Combined Raman and ^{51}V NMR studies suggest that the dehydrated surface vanadium oxide phases are present as a monoxo tetrahedral vanadate species (Raman band in the 1026–1038 cm^{-1} region) and a polymeric tetrahedral metavanadate species (Raman band at ca. 900 cm^{-1}) [51].

In situ Raman studies on Al_2O_3, TiO_2, and SiO_2-supported MoO_3 and WO_3 catalysts also exhibit Raman shifts of the surface molybdenum oxide (from ca. 950 to 985–1012 cm^{-1}) [52–54] and the surface tungsten oxide (from ca. 960 to 1010–1027 cm^{-1}) [52,55–57] phases due to dehydration of the surface metal oxide phases. Two types of the surface molybdenum oxide (tungsten oxide) species on alumina were identified: a highly distorted octahedral MO_6 (WO_6) structure with one terminal bond and a moderately distorted octahedral MO_6 (WO_6) structure with either one or two terminal bonds [58]. For the CrO_3/Al_2O_3 system, a highly distorted tetrahedral CrO_4 species (Raman band at ca. 1005 cm^{-1}) and a polymeric tetrahedral CrO_4 species (Raman band at ca. 880 cm^{-1}) are present [59]. In general, the relative Raman intensity of the two dehydrated metal oxide species (V_2O_5, MoO_3, WO_3, and CrO_3) on alumina depends on the metal oxide loading, and the ratio of the surface polymeric species to the surface monomeric species increases with increasing metal oxide loading. However, the dehydrated metal oxide species (V_2O_5, MoO_3, WO_3, and CrO_3) on the niobia support possessing Raman bands in the 890–956 cm^{-1} region appear to be stronger for the surface modified niobium oxide catalysts (see Table 2) compared to those on alumina. This suggests that metal oxides preferably form a polymeric structure on the niobia support or that metal oxides strongly interact with niobia to form mixed oxide compounds.

The Raman shifts of the dehydrated surface phosphate (ca. 950 to ca. 1004 cm^{-1}) and sulfate (ca. 920 to ca. 1001 cm^{-1}) species suggest the surface tetrahedral PO_4 and SO_4 species are present on niobia. The study of Saur et al. [60] on the sulfated alumina and titania catalysts suggested that the dehydrated surface sulfate species possess a $[MO-]_3S{=}O$ structure (M = Al or Ti), and convert to a $[MO-]_2S(=O)(-OH)$ structure upon hydration which accounts

for the presence of the Brønsted acidity. The molecular structures of the dehydrated surface phosphate species on the alumina and titania supports were determined by Hardcastle and Wachs [39] to possess a metaphosphate structure (a linear PO_4 polymer). A strong and broad Raman band at ca. 932 cm^{-1}, observed for the dehydrated 5 wt.-% SO_4/Nb_2O_5 sample, indicates that sulfates interact with the niobia support to form a mixed Nb–S–O compound which is not perturbed upon dehydration treatments.

Acidity measurements

The nature of Lewis acid and Brønsted acid surface sites present for bulk $Nb_2O_5 \cdot nH_2O$ is dependent on the calcination temperature as shown in Table 3. Acidity measurements indicate that considerable Lewis and Brønsted acid surface sites are present on hydrated niobium oxide when it is activated at 200°C. The surface acidic sites, however, are eliminated at high-temperature treatment (500°C) due to loss in surface area, removal of water, and crystallization of the hydrated niobium oxide structure. These results are consistent with Tanabe's [9] acidity studies on hydrated niobium oxide.

Comparison of the acidic properties of the surface modified niobium oxide catalysts (see Table 3) with those of bulk niobium oxide (500°C) reveals that the deposition of the surface metal oxide or acid species on the niobia support generally retains a considerable amount of Lewis and Brønsted acid surface sites after high-temperature treatment (500°C). The 1 wt.-% V_2O_5/Nb_2O_5 and 1 wt.-% P_2O_5/Nb_2O_5 samples contain a high concentration of surface acid sites,

TABLE 3

Acidic properties of surface modified niobium oxide catalysts
All surface modified niobium oxide catalysts were calcined at 500°C

Catalyst	Amount of LAS[a] {μmol/g[μmol/(m²)]}	A_{des}/A_0[b]	Amount of BAS[a] (μmol/g)
Niobia (act. 200°C)	152 [1.26]	0.33	57
Niobia (cal. 500°C)	0	0	0
1% Re_2O_7/Nb_2O_5	24 [0.60]	0	8
1% CrO_3/Nb_2O_5	39 [0.52]	0	5
1% WO_3/Nb_2O_5	56 [0.80]	0	26
1% MoO_3/Nb_2O_5	12 [0.23]	0	0
1% V_2O_5/Nb_2O_5	106 [1.09]	0.06	46
1% P_2O_5/Nb_2O_5	132 [1.15]	0.34	36
1% SO_4^{2-}/Nb_2O_5	34 [0.36]	0.09	14

[a]LAS: Lewis acid site; BAS; Brønsted acid site.
[b]A_{des}/A_0: the ratio of the IR intensities of 1450 cm^{-1} after and before desorption.

and the 1 wt.-% MoO_3/Nb_2O_5 sample contains a low concentration of surface acid sites. The high surface area and stabilization of amorphous niobia phase (Raman band at ca. 650 cm^{-1}) in the 1 wt.-% V_2O_5/Nb_2O_5 and 1 wt.-% P_2O_5/Nb_2O_5 systems after the 500°C temperature treatments result in the high surface acid sites. However, the MoO_3/Nb_2O_5 system is not stable to high-temperature treatment (500°C), and the phase transformation from amorphous Nb_2O_5 (Raman band at ca. 650 cm^{-1}) to TT–Nb_2O_5 (Raman band at ca. 690 cm^{-1}) [61] results in a low concentration of surface acid sites. The strength of surface Lewis acid sites on 1 wt.-% P_2O_5/Nb_2O_5 is greater than that on 1 wt.-% V_2O_5/Nb_2O_5 due to a high A_{des}/A_0 ratio similar to bulk Nb_2O_5 activated at 200°C (A_0 and A_{des} are the intensities of PyL band before and after desorption, respectively, and the desorption procedures are performed at 350°C for 15 min). Thus, the surface acidity of the surface modified niobium oxide catalysts also depends on the nature of metal oxides.

The presence of Lewis acid surface sites can be explained and predicted by Connell and Dumesic's [62] model for the supported metal oxides on oxide supports. The model successfully explains the creation of Lewis acid surface sites for supported metal oxides on SiO_2 [63]. It assumes that the formal charge of the deposited cations is balanced by the coordinating surface lattice oxygen ions, and that a cation is coordinatively undersaturated if it has a coordination number that is lower than silicon ions have in SiO_2. The application of Connell and Dumesic's model to the systems in this study leads to the predictions that Lewis acid surface sites will be present on all these systems due to the unbalanced formal charge of the deposited cations, and is also consistent with the pyridine adsorption IR measurements in Table 3. The predictions of Brønsted acid surface sites can not be achieved by applying the models of Tanabe et al. [64] or Kataaoka and Dumesic [65], since these models are unable to predict the simultaneous presence of both Lewis and Brønsted acid sites. The presence of new Brønsted acid surface sites can be explained by the retained surface hydroxyl groups on niobia which become sufficiently acidic to protonate pyridine. However, the formation of new surface hydroxyl groups on depositing metal oxides or acids can not be excluded [16].

Catalysis studies

The surface chemistry of the surface modified niobium oxide catalysts were probed with the methanol oxidation reaction because of its ability to discriminate between surface acid sites, formation of dimethyl ether (CH_3OCH_3), surface redox sites, formation of formaldehyde (HCHO) and methyl formate ($HCOOCH_3$), and surface basic sites, formation of $CO+CO_2$. The activity for the methanol oxidation reaction over bulk Nb_2O_5 dramatically decreases with increasing calcination temperature due to the formation of large particles of crystalline Nb_2O_5 and the loss of surface area during thermal treatments [66].

Consequently, bulk Nb_2O_5 (500°C) possesses a low reactivity towards methanol oxidation, but the high CH_3OCH_3 selectivity indicates that bulk Nb_2O_5 possesses a high concentration of surface acid sites (see Table 4).

The influence of the surface metal oxide and acid species on the methanol oxidation catalytic activity and selectivity over the surface modified niobium oxide catalysts with low loading (1 wt.-%) is also presented in Table 4. The surface phosphate and sulfate species on niobia increase the methanol oxidation activity and exhibit 100% CH_3OCH_3 selectivity. The WO_3/Nb_2O_5 system is somewhat less active for this reaction. The surface chromium, rhenium, vanadium and molybdenum oxide species enhance the redox sites on niobia to produce higher selectivity of HCHO, and the V_2O_5/Nb_2O_5 system possesses the highest activity among these catalysts.

The influence of the V_2O_5 concentration on the catalytic properties of the V_2O_5/Nb_2O_5 system, shown in Table 5, is related to the molecular structures of the vanadia species present on the surface. The first ca. 2 wt.-% vanadium oxide is well dispersed on niobia and forms an active surface vanadium oxide species with corresponding Raman band at ca. 1033 cm^{-1} which result in a maximum reactivity and high HCHO selectivity. Thus, the surface acid sites on niobia are replaced by the active vanadium oxide species which possess surface redox sites. Above ca. 2 wt.-% V_2O_5 loading, the presence of a new VO_4 species with corresponding Raman band at ca. 930 cm^{-1}, which are stabilized by the niobia support, results in the decrease of the catalytic activity. The dramatic decrease of the catalytic activity and the absence of V_2O_5 crystallite at high V_2O_5 loadings suggest that V_2O_5 is probably incorporated into the Nb_2O_5 support to form a solid solution.

Recent studies on the supported vanadium oxide catalysts revealed that the

TABLE 4

The catalytic properties of the methanol oxidation reaction over surface modified niobium oxide catalysts
All samples were calcined at 500°C

Catalysts	Activity {mmol/(g)(h) [mmol/(m^2)(h)]}	Selectivity[a]			
		HCHO	CH_3OCH_3	$(CH_3O)_2CH_2$	$CO+CO_2$
Nb_2O_5	5.8 [0.145]	5	95	-	-
1% P_2O_5/Nb_2O_5	36.2 [0.315]	-	100	-	-
1% SO_4^{2-}/Nb_2O_5	32.0 [0.340]	-	100	-	-
1% CrO_3/Nb_2O_5	41.0 [0.530]	45.3	46.9	4.5	1.0
1% WO_3/Nb_2O_5	10.7 [0.152]	-	98.3	-	1.7
1% Re_2O_7/Nb_2O_5	8.0 [0.199]	30.4	58.3	5.5	5.8
1% MoO_3/Nb_2O_5	15.0 [0.283]	21.8	69.2	7.5	1.5
1% V_2O_5/Nb_2O_5	74.2 [0.757]	61.4	35.2	-	3.4

[a] $HCOOCH_3 = 100 - [HCHO + CH_3OCH_3 + (CH_3O)_2CH_2 + (CO+CO_2)]$.

TABLE 5

The catalytic properties of the methanol oxidation reaction over the V_2O_5/Nb_2O_5 system

Catalyst V_2O_5/Nb_2O_5	TON[a]	Selectivity		
		HCHO	CH_3OCH_3	$CO+CO_2$
0% V_2O_5	0.0013[b]	5	95	-
1% V_2O_5	0.194	61.4	35.2	3.4
2% V_2O_5	0.621	90	6.5	3.5
3% V_2O_5	0.586	91.6	4.6	3.8
4% V_2O_5	0.452	93.5	2.5	4.0
5% V_2O_5	0.152	74.2	19.8	6.0
6% V_2O_5	0.154	82.1	11	6.9
7% V_2O_5	0.117	83.2	10.5	6.3
10% V_2O_5	0.097	79.8	15.5	4.7
15% V_2O_5	0.051	81.5	13.2	5.3

[a]TON: (number of CH_3OH converted) per V atom per s.
[b]TON: (number of CH_3OH converted) per Nb atom per s.

same vanadium oxide species possessing one terminal V=O bond and three V–O-support bonds, with corresponding V=O Raman band at ca. 1030 cm^{-1}, preferentially exists on the SiO_2, Nb_2O_5, TiO_2, Al_2O_3, and ZrO_2 supports at low vanadium oxide surface coverages [7]. The TON of the methanol oxidation of the supported vanadium oxide catalysts has the following order: 1% V_2O_5/ZrO_2 ($2.3 \cdot 10^0$) > 1% V_2O_5/TiO_2 ($1.8 \cdot 10^0$) > 1% V_2O_5/Nb_2O_5 ($7 \cdot 10^{-1}$) > 1% V_2O_5/Al_2O_3 ($2.6 \cdot 10^{-2}$) > 1% V_2O_5/SiO_2 ($2 \cdot 10^{-3}$). In the previous study, the niobia support was treated at 500°C before the impregnation of vanadium oxide. The dramatic influence of the oxide support upon the reactivity of the supported vanadium oxide catalysts is related to the surface oxide–support interactions. Consequently, the V–O–M (M = Zr, Ti, and Nb) interactions possess a higher activity than the V–O–M (M = Al and Si) interactions for the supported vanadium oxide catalysts. In the present study, the TON for methanol oxidation over the 1% V_2O_5/Nb_2O_5 sample ($1.9 \cdot 10^{-1}$), where the niobia support was calcined at 500°C after the impregnation of vanadia, has the same order of magnitude as the 1% V_2O_5/Nb_2O_5 sample ($7 \cdot 10^{-1}$), where the niobia support was treated at 500°C before the impregnation of vanadia. The 35.2% selectivity of CH_3OCH_3 in the first 1% V_2O_5/Nb_2O_5 sample results from the original surface acid sites on the niobia support. Thus, the reactivity of the surface modified niobium oxide catalysts strongly depend on the nature of metal oxides as well as the metal oxide loading.

CONCLUSIONS

Metal oxides (Re_2O_7, CrO_3, WO_3, MoO_3, and V_2O_5) and acids (P_2O_5 and SO_4^{2-}) form a two-dimensional overlayer on the niobia support, and the molec-

ular structures of these surface metal oxide and acid species under ambient conditions are similar to the ReO_4^{1-}, $Cr_3O_{10}^{2-}$, $W_{12}O_{40}^{8-}$, $Mo_8O_{26}^{4-}$, $V_{10}O_{28}^{4-}$ and $H_2PO_4^{1-}$, HSO_4^{1-} species present in acidic solutions. Upon dehydration, only one dehydrated surface ReO_4 species is present on niobia. For the CrO_3, WO_3, MoO_3, and V_2O_5 supported on niobia, two dehydrated surface metal oxide species: highly distorted and slightly distorted structures, are present. Both highly distorted PO_4 (SO_4) and slightly distorted PO_4 (SO_4) are also observed on niobia. Acidity and BET studies on the surface modified niobium oxide catalysts reveal that the presence of the surface metal oxide or acid species retains the surface acidic properties and surface area of niobia during high calcination temperatures (500°C). The 1% V_2O_5/Nb_2O_5 and 1% P_2O_5/Nb_2O_5 samples contain a high surface acid site concentration as well as surface area, and the strength of surface Lewis acid sites on 1% P_2O_5/Nb_2O_5 is stronger than that of the other systems. In addition, the surface vanadium, molybdenum, and chromium oxide sites on niobia behave as redox sites and the surface tungsten oxide, phosphate, and sulfate sites on niobia are acid sites during methanol oxidation reaction. The weak interaction between the surface rhenium oxide species and the niobia support results in volatilization of surface rhenium oxide during methanol oxidation and a corresponding low activity.

ACKNOWLEDGEMENT

Financial support for this work by Niobium Products Company, Inc. is gratefully acknowledged.

REFERENCES

1 T. Iizuka, T. Tanaka and K. Tanabe, J. Mol. Catal., 17 (1982) 381.
2 M.A. Vannice and S.J. Tauster, U.K. Patent 2 006 261 (1978).
3 E.I. Ko, J.M. Hupp and N.J. Wagner, J. Catal., 86 (1984) 315.
4 J.M. Jehng and I.E. Wachs, Catal. Today, 8 (1990) 37.
5 Y.S. Jin, A. Ouqour, A. Auroux and J.C. Vedrine, Study in Surf. Sci. Catal., 48 (1989) 525.
6 Y. Kera and T. Kawashima, Bull. Chem. Soc. Jpn., 61 (1988) 1491.
7 G. Deo and I.E. Wachs, J. Catal., 129 (1991) 307.
8 K. Tanabe, Heterogeneous Catalysis, Texas A & M Univ. Press, 1984, p. 71.
9 K. Tanabe, Mat. Chem. and Phys., 17 (1987) 217.
10 Z. Chen, T. Iizuka and K. Tanabe, Chem. Lett., (1984) 1085.
11 K. Ogasawara, T. Iizuka and K. Tanabe, Chem. Lett., (1984) 645.
12 T. Iizuka, K. Ogasawara and K. Tanabe, Bull. Chem. Soc. Jpn., 56 (1983) 2927.
13 T. Hanaoka, K. Takeuchi, T. Matsuzaki and Y. Sugi, Catal. Today, 8 (1990) 123.
14 I.E. Wachs, F.D. Hardcastle and S.S. Chan, Spectroscopy, 1 (1986) 30.
15 J. Datka, J. Chem. Soc. Farady Trans. 1, 77 (1981) 2877.
16 J. Datka, A.M. Turek, J.M. Jehng and I.E. Wachs, J. Catal., in press.
17 J.M. Jehng and I.E. Wachs, Chem. Mater., 3 (1991) 100.
18 L.L. Murrell and D.C. Grenoble, U.S. Patent 4 415 480 (1983).

19 I.E. Wachs, J.M. Jehng and F.D. Hardcastle, Solid State Ionics, 32/33 (1989) 904.
20 S. Okazaki and A. Kurosaki, Catal. Today, 8 (1990) 113.
21 R.L. Martins, W.J. Schitine and F.R. Castro, Catal. Today, 5 (1989) 483.
22 S. Okazaki, T. Iizukz and S. Kado, Brazilian Patent PI 8503415 (1985).
23 F.D. Hardcastle and I.E. Wachs, J. Mol. Catal., 46 (1988) 15.
24 F. Gonzalez-Vichez, W.P. Griffith, J. Chem. Soc., Dalton Trans., (1972) 1416.
25 F.D. Hardcastle and I.E. Wachs, J. Mol. Catal., 46 (1988) 173.
26 C.F. Baes Jr. and R.E. Mesmer, The Hydrolysis of Cations, Wiley, New York, 1976, p. 211.
27 M.A. Vuurman, D.J. Stufkens, O. Oskam, J.A. Moulijn and F. Kapteijn, J. Mol. Catal., 60 (1990) 83.
28 S.S. Chan, I.E. Wachs, L.L. Murrell and N.C. Dispenziere, J. Catal., 92 (1985) 1.
29 M.A. Vuurman, I.E. Wachs and A.M. Hirt, J. Phys. Chem., 95 (1991) 9928.
30 T. Machej, J. Haber, A.M. Turek and I.E. Wachs, Appl. Catal., 70 (1991) 115.
31 J.M. Stencel, Raman Spectroscopy for Catalysis, Van Nostrand Reinhold, New York, 1990.
32 G. Deo and I.E. Wachs, J. Phys. Chem., 95 (1991) 5889.
33 H. Eckert and I.E. Wachs, in preparation.
34 G. Deo, F.D. Hardcastle, M. Richards, A.M. Hirt and I.E. Wachs, ACS Symp. Ser., 437 (1990) 317.
35 J. Davi, D. Tinet, J.J. Fripiat, J.M. Amarilla, B. Casal, E. Ruiz-Hitzky, J. Mater. Res., 6 (1991) 393.
36 F.D. Hardcastle and I.E. Wachs, J. Phys. Chem., 95 (1991) 5031.
37 A. Kayo, T. Yamaguchi and K. Tanabe, J. Catal., 83 (1983) 99.
38 D.E.C. Corbridge, M.S. Pearson and C. Walling, Topics in Phosphorous Chemistry, Vol. 3, Interscience, New York, 1966, p. 71.
39 F.D. Hardcastle and I.E. Wachs, in preparation.
40 S. Sato, S. Higuchi and S. Tanaka, Appl. Spec., 39 (1985) 822.
41 G. Busca, G. Ramis, V. Lorenzelli, R.F. Rossi, A.L. Ginestra and P. Patrono, Langmuir, 5 (1989) 993.
42 G.A. Park, Chem. Rev., 65 (1965) 177.
43 G.A. Park, Adv. Chem. Ser., 61 (1967) 121.
44 F.J. Gil-Llamblas, A.M. Escudey, J.C.G. Fierro and A.C. Agudo, J. Catal., 95 (1985) 520.
45 S.S. Chan, I.E. Wachs, L.L. Murrell, L. Wang and W.K. Hall, J. Phys. Chem., 88 (1984) 5831.
46 M.A. Vuurman, I.E. Wachs, D.J. Stufkens and A. Oskam, J. Mol. Catal., submitted for publication.
47 G. Deo, H. Eckert and I.E. Wachs, Prep. Amer. Chem. Soc. Div. Petrol. Chem., 35 (1990) 16.
48 G. Deo, M. Vuurman and I.E. Wachs, in preparation.
49 G.T. Went, S.T. Oyama and A.T. Bell, J. Phys. Chem., 94 (1990) 4240.
50 S.T. Oyama, G.T. Went, K.B. Lewis, A.T. Bell and G. Somarjai, J. Phys. Chem., 93 (1989) 6786.
51 I.E. Wachs, J. Catal., 124 (1990) 570.
52 T. Machej, J. Haber, A.M. Turek and I.E. Wachs, in preparation.
53 J.M. Stencel, L.E. Makovsky, T.A. Sarkus, J. de Vries, R. Thomas and J. Moulijn, J. Catal., 90 (1984) 314.
54 J.M. Stencel, J.R. Diehl, J.R. D'Este, L.C. Makovsky, L. Rodrigo, K. Marcinkowska, A. Adnot, P.C. Roberge and S. Kaliaguine, J. Phys. Chem., 90 (1986) 4739.
55 S.S. Chan, I.E. Wachs, L.L. Murrell and N.C. Dispenziere, J. Catal., 92 (1985) 1.
56 S.S. Chan, I.E. Wachs and L.L. Murrell, J. Catal., 90 (1984) 150.
57 J.M. Stencel, L.E. Makovsky, J.R. Diehl and T.A. Sarkus, J. Raman Spectrosc., 15 (1984) 282.

58 F.D. Hardcastle, Ph.D. Dissertation, Lehigh University, University Microfilms International, Ann Arbor, MI, 1990.
59 M.A. Vuurman and I.E. Wachs, in preparation.
60 O. Saur, M. Bensitel, A.B. Mohammed Saad, J.C. Lavalley, C.P. Tripp and B.A. Morrow, J. Catal., 99 (1986) 104.
61 J.M. Jehng and I.E. Wachs, unpublished results.
62 G. Connell and J.A. Dumesic, J. Catal., 102 (1986) 216.
63 G. Connell and J.A. Dumesic, J. Catal., 105 (1987) 285.
64 K. Tanabe, T. Sumiyoshi, K. Shibata, T. Kiyoura and J. Kitagawa, Bull. Chem. Soc. Jpn., 47 (1974) 1064.
65 T. Kataaoka and J.A. Dumesic, J. Catal., 112 (1988) 66.
66 J.M. Jehng, Ph.D. Dissertation, Lehigh University, University Microfilms Int., Ann Arbor, MI, 1990.